

MODELING AND SIMULATION OF WALL-FLOW DIESEL PARTICULATE FILTER DURING LOADING AND REGENERATION

By

Zhenhua Guo

A DISSERTATION

Presented to the Faculty of

The Graduate College at the University of Nebraska

In Partial Fulfillment of Requirements

For the Degree of Doctor of Philosophy

Major: Engineering

Under the Supervision of Professor Zhaoyan Zhang

Lincoln, Nebraska

November, 2006

UMI Number: 3236910

PREVIEW

UMI[®]

UMI Microform 3236910

Copyright 2006 by ProQuest Information and Learning Company.
All rights reserved. This microform edition is protected against
unauthorized copying under Title 17, United States Code.

ProQuest Information and Learning Company
300 North Zeeb Road
P.O. Box 1346
Ann Arbor, MI 48106-1346

**MODELING AND SIMULATION OF WALL-FLOW DIESEL PARTICULATE
FILTER DURING LOADING AND REGENERATION**

Zhenhua Guo, Ph.D.

University of Nebraska, 2006

Adviser: Zhaoyan Zhang

The advent of tightened diesel emission regulations has led to the development and implementation of various diesel in-cylinder controls and after-treatment devices. As the most promising after-treatment device in reducing particulate emission from diesel engines, the diesel particulate filter (DPF) was developed in the 1980s and has undergone notable improvements. The objective of this dissertation is to explore complicated physical processes in the DPF during loading and regeneration.

In the 1-D model, quasi-steady state conservations of mass and momentum are solved by a shooting method coupled with a Runge-Kutta method. A filtration model based on unit collector filtration theory is used to determine transient filtration behaviors of the porous wall. Transient conservations of energy are solved with fully implicit finite difference method to find the temperature field.

The major challenge with DPF is the uncertainty of the regeneration process. The exothermic soot oxidation during regeneration leads to sharp rise in local temperature and temperature gradient, which makes the DPF susceptible to melting and cracking. As an

extension of the 1-D model, a quasi 3-D model is developed to locate hot spots in the DPF. The 3-D Navier-Stokes equations are solved using order of magnitude analysis and integral method. The 3-D transient conservation of energy is solved by a modified Alternative-Direction-Implicit (ADI) method to find the temperature distribution, which enables further numerical simulation of thermal stress.

A displacement-based finite element method is employed to solve for the 3-D thermal stress induced by high temperature and temperature gradient during DPF regeneration. This finite element model is self-contained and independent of any commercial package. It includes functions of meshing body, assembling global stiffness matrix and force vector, solving final equilibrium equations and post-processing.

Finally, parametric studies are carried out with these three models to investigate the impact of DPF geometric designs on performance. Primary attention is paid to pressure drop, peak temperature and thermal stress, which are associated with diesel thermal efficiency and potential DPF failure due to melting and cracking.

ACKNOWLEDGEMENT

During the period I have been working for this dissertation, a lot of people helped me and supported me in a variety of ways. I am indebted to all of them. Here, I express my special thanks to them.

I would like to express my sincere gratitude and appreciation to my advisor, Dr. Zhaoyan Zhang, for providing me with the unique opportunity to work in the research area of diesel particulate filter, for his expert guidance and mentorship, and for his encouragement and support at all levels.

I would like to thank Dr. John Barton and Dr. Kevin Cole for reading this dissertation and offering constructive comments. Also, I will wish to acknowledge my appreciation to other committee members, Dr. David Lou, Dr. George Gogos and Dr. Jiashi Yang, for providing assistance and thought-provoking ideas throughout my research.

Finally, I would like to thank my family for their life-long love and support. I especially owe much to my wife for offering her invaluable encouragement to help me debug the code during numerical simulation and to make this work a joy. Without them, this work could not have been completed.

CONTENTS

ACKNOWLEDGEMENT	i
CONTENTS	ii
LIST OF TABLES	v
LIST OF FIGURES	vi
NOMENCLATURE	x
CHAPTER 1: INTRODUCTION	1
1.1 Diesel Particulate Filter	1
1.2 Literature Review	7
1.2.1 Experimental Work	7
1.2.2 Theoretical Analyses and Numerical Simulations	10
1.2.2.1 Single Channel Model	11
1.2.2.2 Whole Scale Model	14
CHAPTER 2: 1-D MODELING AND SIMULATION OF DPF	17
2.1 Mathematical Formulations	17
2.1.1 Conservation of Mass and Momentum	17
2.1.2 Transient Filtration Model	20
2.1.3 Conservation of Energy	24
2.2 Numerical Methods	26
2.2.1 Flow Field	26
2.2.2 Temperature Field	27
2.3 Model Validation and Calibration	28
2.4 Results and Discussions	37
2.5 Conclusions	45
CHAPTER 3: QUASI 3-D MODELING AND SIMULATION OF DPF	47
3.1 Mathematical Models	47

3.1.1 Flow Field	47
3.1.2 Temperature Field.....	50
3.2 Numerical Schemes.....	52
3.2.1 Flow Field Solver with Integral Method.....	52
3.2.2 Temperature Field Solver with ADI Method	55
3.3 Model Validation.....	56
3.4 Results and Discussions	59
3.5 Conclusions	64
CHAPTER 4: 3-D TRANSIENT ELASTIC THERMAL STRESS	
FIELD DURING DPF REGENERATION	65
4.1 Fundamentals of Thermal Stress.....	65
4.1.1 Assumptions	65
4.1.2 Theory of Thermo-Elasticity	66
4.2 Finite Element Method	69
4.2.1 General Description of Finite Element Method	69
4.2.2 Shape Functions.....	70
4.2.3 Stiffness Matrix and Force Vector	72
4.2.4 Numerical Integration.....	74
4.2.5 Solution of Final Equilibrium Equation	75
4.3 DPF Thermal Stress Analysis with Finite Element Method.....	76
4.3.1 Computational Domain and Boundary Conditions	77
4.3.2 Effective Material Properties	78
4.3.3 Temperature Interpolation	78
4.4 Model Validation.....	79
4.5 Results and Discussions.....	82
4.6 Conclusions	85
CHAPTER 5: OPTIMIZATION OF DPF PARAMETRIC DESIGN	87

5.1 Constant Filtration Volume	87
5.2 Constant Cell Density.....	90
5.3 Conclusions	91
CHAPTER 6: CONCLUSIONS	94
CHAPTER 7: FUTURE WORK	96
REFERENCES	97
APPENDIX A: NONDIMENSIONALIZATION OF NAVIER-STOKES	
EQUATIONS	105
APPENDIX B: IMPLEMENTATION OF INTEGRAL METHOD	108

PREVIEW

LIST OF TABLES

Table 2.1: Particulate size distribution

Table 2.2: Input data for DPF#1

Table 2.3: Input data for DPF#2

Table 2.4: Input data for DPF#3

Table 2.5: Reaction kinetics for particulate oxidation

Table 4.1: Gaussian points and weights for Gaussian quadrature

Table 4.2: Input data for validation of thermal stress model

LIST OF FIGURES

Figure 1.1: A finished DPF and alternate plugged channel patterns

Figure 1.2: Gas flow in DPF

Figure 1.3: Classification of DPF system by regeneration strategy

Figure 2.1: Schematic of DPF channels. (a) side view, (b) front view

Figure 2.2: Types of filtration. (a) depth filtration, (b) cake filtration

Figure 2.3: Idealized spherical unit collector and its three filtration conditions

Figure 2.4: Comparison of normalized axial velocities in inlet and outlet channels between numerical simulation and analytical solution for a clean DPF

Figure 2.5: Comparison of normalized pressure drop across porous wall between numerical simulation and analytical solution for a clean DPF

Figure 2.6: Exhaust exit temperature predicted by 1-D and zero-dimensional models during heating up process of a clean DPF

Figure 2.7: Predicted pressure drop by numerical simulation against experimental data during the loading process of a clean uncatalyzed DPF

Figure 2.8: Comparisons of pressure drop and retained particulate mass between numerical simulation and experimental data during a controlled regeneration

Figure 2.9: Comparison of wall temperature in the middle of DPF between numerical simulation and experiment data during a controlled regeneration

Figure 2.10: Particulate layer thickness distribution at the end of two loading processes

Figure 2.11: Wall velocity distribution at the end of two loading processes

Figure 2.12: Pressure drop vs. time during loading process for a clean catalyzed DPF

Figure 2.13: Particulate layer thickness distribution at three loading instants

Figure 2.14: Impact of DPF length on total pressure drop for a clean DPF

Figure 2.15: Histories of porous wall temperature at the end of DPF for three different initial soot mass loadings

Figure 2.16: Pressure drops vs. time for three different initial soot mass loadings

Figure 2.17: Particulate layer thickness distributions after regeneration for three different initial soot mass loadings

Figure 3.1: Computational domain for flow and temperature fields

Figure 3.2: Comparisons of average x -component of flow velocities between quasi 3-D simulation and analytical solution for a clean DPF

Figure 3.3: Average porous wall temperature predicted by 3-D and 1-D numerical models during DPF heating-up process

Figure 3.4: Comparison of porous wall temperature in the middle of DPF between experimental measurement and 3-D numerical simulation during a controlled regeneration

Figure 3.5: Contour plots of flow and temperature fields in the middle of DPF. (a) x -component of velocity; (b) y -component of velocity; (c) z -component of velocity; (d) temperature

Figure 3.6: Maximum temperature differences between four points under various particulate loadings during regeneration

Figure 3.7: Instants when maximum temperature gradient and maximum temperature occur under various particulate loadings during regeneration

Figure 3.8: Contour plots of temperature field at the end of DPF under two different initial particulate loadings. (a) $m=220$ g, maximum temperature gradient; (b) $m=220$ g, maximum temperature; (c) $m=240$ g, maximum temperature gradient; (d) $m=240$ g, maximum temperature

Figure 4.1: Mapping between hexahedron element in global coordinate system and brick element in isoparametric coordinate system

Figure 4.2: Storage of symmetric banded global stiffness matrix in finite element method

Figure 4.3: Geometry of DPF porous wall for 3-D thermal stress analysis

Figure 4.4: 3rd principal thermal stress predicted by 3-D model

Figure 4.5: 3rd principal thermal stress predicted by ANSYS

Figure 4.6: Comparison of 3rd principal thermal stress at the end of DPF between 3-D model and ANSYS

Figure 4.7: Back view of 3rd principal thermal stress when the maximum temperature gradient occurs for initial soot loading at 220g

Figure 4.8: Back view of 3rd principal thermal stress when maximum temperature occurs for initial soot loading at 220g

Figure 4.9: Back view of 3rd principal thermal stress when maximum temperature gradient occurs for initial soot loading at 240g

Figure 4.10: Back view of 3rd principal thermal stress when maximum temperature occurs for initial soot loading at 240g

Figure 4.11: Variation of maximum 3rd principal thermal stress with initial soot mass loading

Figure 5.1: Pressure drops during particulate loading for five different DPF geometries with constant filtration volume

Figure 5.2: Porous wall temperatures during regeneration for five different DPF geometries with constant filtration volume

Figure 5.3: Maximum 3rd principal thermal stresses for five different DPF geometries with constant filtration volume

Figure 5.4: Pressure drops during particulate loading for five different DPF geometries with constant cell density

Figure 5.5: Porous wall temperatures during regeneration for five different DPF geometries with constant cell density

Figure 5.6: Maximum 3rd principal thermal stresses for five different DPF geometries with constant cell density

NOMENCLATURE

Roman

A :	pre-exponential factor
b :	unit cell diameter
C_f :	friction coefficient
c_p :	specific heat
d_{c0} :	diameter of clean unit collector
d_{pore} :	mean pore size of porous wall
D :	channel width
D_i :	diameter of diesel particulate filter
$[D]$:	symmetric material matrix
E :	Young's modulus
\vec{F} :	force vector
E_{act} :	activation energy
G	shear modulus
H :	characteristic dimension in 3-D computational domain
H_{reac} :	enthalpy of formation
hbw :	half band width of global stiffness matrix
k :	permeability
$[K]$:	stiffness matrix

L :	length of diesel particulate filter
m :	mass
n :	number of nodes
N :	number of inlet channels
$[O_2]$:	oxygen mass concentration in exhaust gas
P :	exhaust gas pressure
\vec{Q} :	displacement vector
Re :	Reynolds number
R_u :	universal gas constant
RR :	reaction rate of particulate oxidation
ST :	source term
T :	temperature
T_{in} :	exhaust entrance temperature
u, v, w :	components of velocity
$\underline{u}, \underline{v}, \underline{w}$:	components of displacement
u_{in} :	exhaust entrance velocity
u_w :	mean wall velocity
U :	maximum axial velocity
W :	thickness
x, y, z :	coordinates in Cartesian system

Greek

α : linear thermal expansion coefficient

β_0 : porosity of clean porous wall

$\vec{\varepsilon}$: strain vector

λ : thermal conductivity

μ : dynamic viscosity

ν : Poisson's ratio

ξ, η, ζ : coordinates in isoparametric system

ρ : density

$\vec{\sigma}$: stress vector

ω : solid fraction

Subscripts

c : catalytic particulate oxidation

f : exhaust gas

i : inlet channel

o : outlet channel

p : particulate matter

s : porous wall

t : thermal particulate oxidation

∞ : exhaust gas condition before entering diesel particulate filter

Superscripts

*

dimensionless quantity

CHAPTER

1

INTRODUCTION

1.1 Diesel Particulate Filter

The global automotive industry is currently facing complex challenges to reduce transportation related environmental impact. Significant reduction in greenhouse emissions from internal combustion engines can be achieved through increased deployment of modern, highly efficient diesel engines, such as common rail direct injection diesel engines. Diesel engines operate at very lean stoichiometry, with air fuel ratio approximately greater than 22. They have good fuel economy, producing less CO₂. It is not uncommon for a diesel engine to have a lifespan of 1 million miles, about 10 times that of the gasoline engine. The diesel fuel and air mixture are highly compressed raising the gas temperature to the point of combustion. Its lean nature results in a cooler combustion with less gaseous CO and HC emissions than its gasoline counterpart. However, the diesel engines emit higher levels of NO_x and particulate emissions due to the presence of excessive oxygen in the fuel/air mixture and the heterogeneous combustion of the fuel/air mixture in the engine chamber.

The NO_x emissions contribute to photochemical smog and respiratory irritation. The particulate matter can penetrate deeply into the lung and is a potential occupational carcinogen of the human respiratory system.

On December 21, 2000 the US Environment Protection Agency (EPA) published emission standards for heavy-duty truck and bus engines for year 2007 and later. The new standards are: particulate matter (PM)-0.01 g/bhp-hr; nitrogen oxides (NO_x)-0.2 g/bhp-hr; and, hydrocarbon (HC)-0.15 g/bhp-hr. Nonroad (off-road) diesel engines, such as farm tractors, excavators, lawn tractors, logging equipments and road graders are regulated separately from the heavy-duty highway engines. In 1994, the first emission standards for new nonroad engines over 37kW were adopted and phased in from 1996-2000 (this phase was designated as Tier 1). By 1998 the Tier 1 regulations also included engines under 37kW. Tier 2 and Tier 3 standards were phased in from 2000-2008. On April 15, 2003 the EPA proposed Tier 4 emission standards for new nonroad diesel engines to be phased in from 2008-2014. The new standards require 90% reductions of PM and NO_x from Tier 3 levels.

The control of particulate and NO_x emissions make the diesel engine manufacturer subject to demanding challenges because the generation mechanisms of these two pollutants are inversely coupled. When the engine operates at lower internal temperature, it produces less NO_x but more particulate emissions. At higher temperature, combustion is more complete, generating less particulate but more NO_x. This is referred to as the NO_x-particulate tradeoff, which makes the in-cylinder control of both pollutants a complicated task. Therefore, compliance with the NO_x and particulate emissions standards will require the implementation of after-treatment devices for one or both pollutants.

The diesel particulate filter (DPF) was developed as a promising after-treatment device for particulate emissions in the 1980s and has undergone notable improvement since. The most common design of DPF is the wall flow monolith. It is a cylindrical ceramic structure with numerous small, parallel channels plugged at the alternate ends. The DPF is manufactured by extrusion from paste of ceramic precursors using precision dies, followed by drying. The dried parts are then cut to the desired length and fired in an oven. Combustible pore precursor substances (polymers and graphite) which may be added to the raw material are oxidized during the firing process, thus creating the pore network in the monolith walls. In the next step of the process, the channel ends are plugged with ceramics and the filters are fired again. Plugged parts are checked for leaks through a diesel exhaust test. If leaking channels are detected, they are plugged with ceramic cement. A finished wall-flow DPF is shown in Figure 1.1. The alternate plugged cell patterns for different cell configurations are clearly visible in the enlarged section.

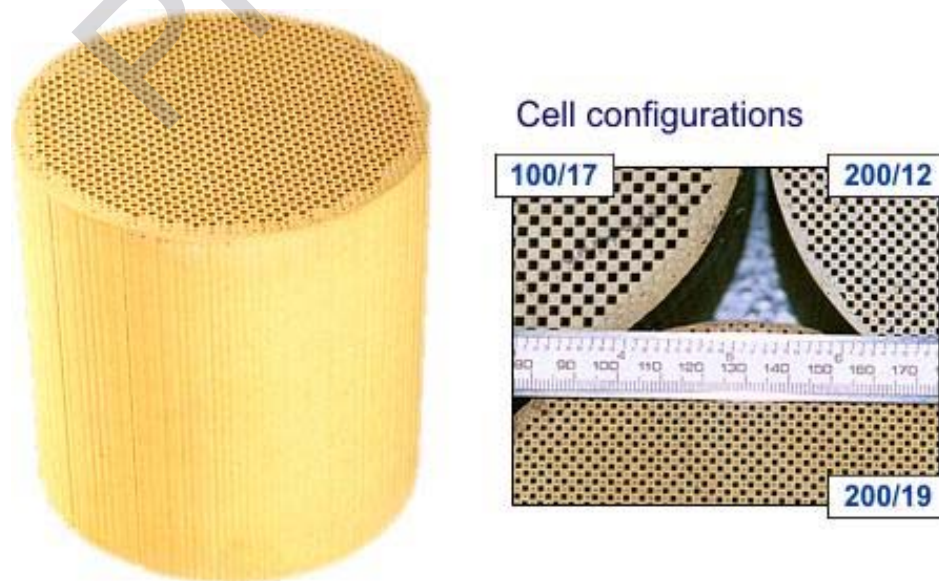


Figure 1.1: A finished DPF and alternate plugged channel patterns

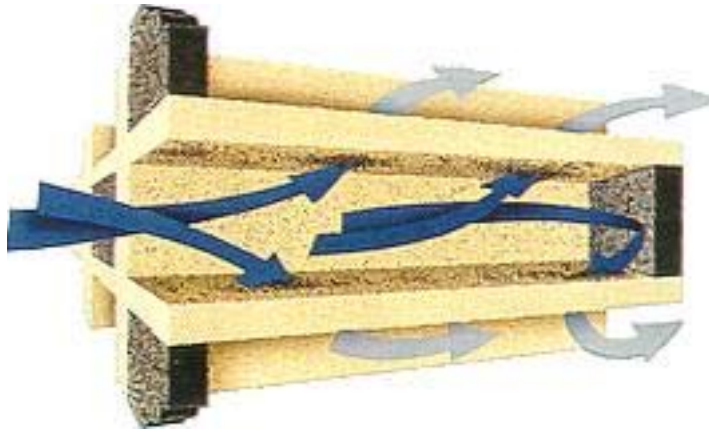


Figure 1.2: Gas flow in DPF (www.dieselnet.com)

The channels plugged at the rear are called inlet channels, and the channels plugged in the front are called outlet channels. As demonstrated in Figure 1.2, exhaust gas entering filter from inlet channels, is forced to pass through the porous wall into the adjoining outlet channels. During this process, the particulate matter is captured inside the porous wall and forms a particulate layer above the wall as well. The collected particulate matters cause the pressure drop across DPF to increase. Excessive pressure drop affects engine performance and penalizes fuel economy. Therefore, after a period of usage, those collected particulate matters have to be removed from the DPF periodically by oxidation to prevent excessive pressure drop in exhaust system. The particulate oxidation process is termed regeneration of the DPF.

The major challenge with DPF is the uncertainty of the regeneration process [1, 2 and 3]. The particulate matter consists mainly of carbonaceous matter. Its heating value is very high and a small amount of particulate matter will release considerable heat during regeneration. If the released heat cannot be removed rapidly from DPF, high temperature

and temperature gradient will occur and may lead to melting and cracking of DPF [4, 5].

Typically, the particulate matter begins to oxidize, when the filter is sufficiently loaded and the inlet exhaust temperature exceeds 550 °C. For typical heavy duty and light duty diesel engines, filter inlet exhaust temperature of 550 °C are rarely obtained even though the engines are operated at full load [6, 7]. Therefore, it is unlikely that the particulate matter collected in the filter will start oxidation under engine regular operating conditions. That problem may be solved by either (a) decreasing the required soot oxidation temperature to a level which can be reached during regular engine operating condition [8] or (b) increasing the temperature in the DPF to the point when deposited soot starts oxidizing [9, 10]. The first approach is used in passive filter systems, the second in active filter systems. A classification of DPF based on the principle of regeneration is shown in Figure 1.3.

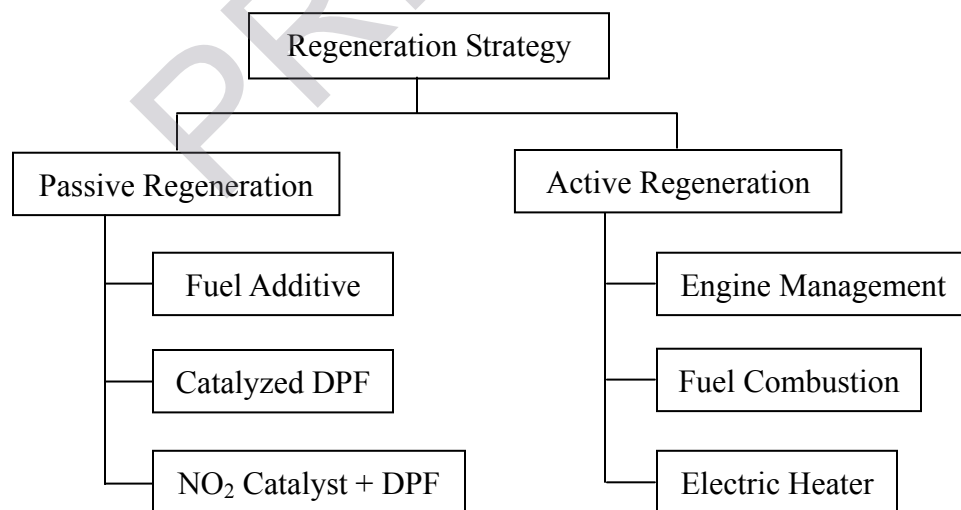


Figure 1.3: Classification of DPF system by regeneration strategy

In passive systems, the soot oxidation temperature is lowered to a level allowing for

auto-regeneration during regular vehicle operation, a task commonly achieved by introducing an oxidation catalyst to the system. The catalyst can promote soot oxidation through two mechanisms [11, 12 and 13]: (a) oxygen mechanism-catalytic oxidation of soot by oxygen; or, (b) nitrogen dioxide mechanism-catalytic oxidation of NO to NO₂, followed by the oxidation of soot by nitrogen dioxide.

With different placement of the catalyst and different system configurations, one of the following approaches or their combination can be utilized: (a) adding a catalyst to the fuel as an additive [14]; (b) coating the porous wall with precise catalyst; or, (c) using NO₂ generating catalyst upstream of the DPF.

The active system triggers regeneration by raising the temperature necessary for soot oxidation through the use of an external energy source. There are two obvious energy sources that are available on vehicle: diesel fuel and electricity. The energy from fuel combustion can be used to increase exhaust gas temperature by either (a) in-cylinder engine management methods, such as late cycle injection of additional fuel quantities, or (b) injection and combustion of fuel in the exhaust gas. If the exhaust gas combustion is used, fuel can be burned in a fuel burner or else oxidized over an oxidation catalyst in a catalytic combustion process. Electric heating can be used in a number of configurations, such as placing an electric heater upstream of the DPF.

Cordierite ($2\text{MgO} \cdot 2\text{Al}_2\text{O}_3 \cdot 5\text{SiO}_2$) and silicon carbide (SiC) are two widely used materials in commercialized DPF. Cordierite DPF, introduced in the mid-1980s on

Mercedes cars sold in California, have been used in numerous applications. With time, cordierite became the most common material in DPF for heavy-duty applications. SiC DPF was introduced in the 1990s. Since that time, nearly all DPFs in European passenger cars contain SiC material. Cordierite is characterized by good thermal shock resistance and lower cost, but it has lower melting temperature. On the contrary, SiC has higher operating temperature limit but lower thermal shock resistance, which makes it susceptible to cracking. The porous wall material is confined to cordierite in this dissertation.

1.2 Literature Review

A considerable number of publications related to this dissertation have appeared in the literature. They deal with experimental, theoretical and numerical studies of the complicated transport processes in the DPF. The literature survey will proceed as follows. In the first section, experimental work with respect to DPF performance will be discussed. It is followed by a review of theoretical analyses and numerical models that have been developed to date.

1.2.1 Experimental Work

Tan et al. [15] carried out experiments to understand the regeneration process in ceramic DPF using a copper fuel additive and to investigate the various conditions that led to DPF regeneration failure. It was found that the copper additive lowered the DPF

regeneration temperature from approximately 550 °C to 375 °C and decreased the time necessary for regeneration. Suresh et al. [16] performed experiments with several commonly used DPF to determine the regeneration efficiency of these filters at different loading conditions. Temperatures inside the DPF were constantly monitored during the experimental runs by using ungrounded inconel K type thermocouples, which were inserted from the outlet channels to their desired positions. The pressure drop across the DPF was measured using pressure taps before and after the filter in the exhaust system.

It was well documented in correlating pressure drop with exhaust flow rate and particulate loading for uncatalyzed DPFs. However, coating catalyst on a DPF may alter the pore micro-structure and results in significantly different pressure drop behavior. Flöerchinger et al. [17] performed pressure drop measurements in an engine dynamometer test cell to explore the impacts of catalyst type and coating technique on pressure drop. A pressure drop model developed and validated for uncatalyzed DPF was extended to make it applicable in predicting pressure drop associated with catalyzed DPF.

Yezerets et al. [18] applied several complementary experimental techniques to investigate kinetics of soot oxidation by O₂ in an attempt to provide accurate data for modeling DPF regeneration process. Good mathematical description of the results was obtained using the hypothesis that reaction order with respect to soot mass was close to unity. Hanamura et al. [19] clarified the combustion mechanism during DPF regeneration through a visualization experiment, using a half-cylindrical wall-flow DPF covered by a